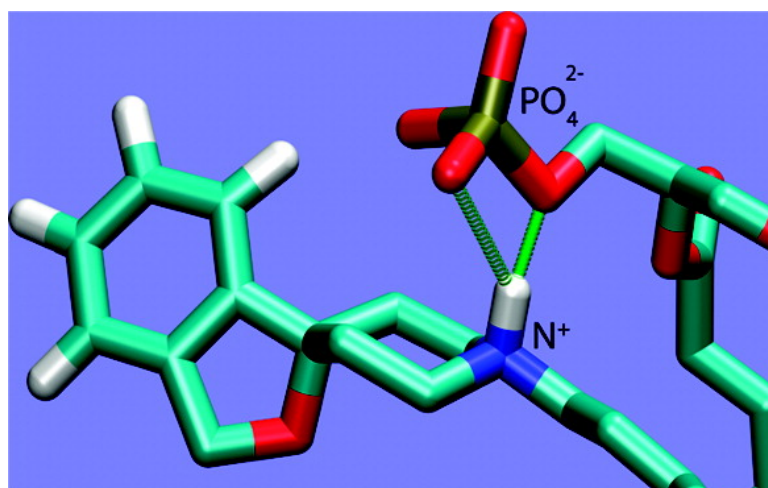Article

# High-Affinity Small Molecule#Phospholipid Complex Formation: Binding of Siramesine to Phosphatidic Acid

Mikko J. Parry, Juha-Matti I. Alakoskela, Himanshu Khandelia, Subramanian Arun Kumar, Marja Ja#a#ttela#, Ajay K. Mahalka, and Paavo K. J. Kinnunen

## More About This Article

Additional resources and features associated with this article are available within the HTML version:

- Supporting Information
- Access to high resolution figures
- Links to articles and content related to this article
- Copyright permission to reproduce figures and/or text from this article

View the Full Text HTML

# High-Affinity Small Molecule−Phospholipid Complex Formation: Binding of Siramesine to Phosphatidic Acid

Mikko J. Parry,[†] Juha-Matti I. Alakoskela,[†] Himanshu Khandelia,[‡] Subramanian Arun Kumar,[§,||] Marja Jäättelä,[⊥] Ajay K. Mahalka,[†] and Paavo K. J. Kinnunen*,[†,‡]

*Helsinki Biophysics & Biomembrane Group, Institute of Biomedicine, University of Helsinki, Finland, MEMPHYS-Center for Biomembrane Physics, University of Southern Denmark, Odense M, Denmark, School of Chemistry, University of Reading, United Kingdom, Nucleic Acids Center, University of Southern Denmark, Odense M, Denmark, and Apoptosis Department, Institute for Cancer Biology, Danish Cancer Society, Copenhagen, Denmark*

Received January 29, 2008; E-mail: paavo.kinnunen@helsinki.fi

**Abstract:** Siramesine (SRM) is a $\sigma-2$ receptor agonist which has been recently shown to inhibit growth of cancer cells. Fluorescence spectroscopy experiments revealed two distinct binding sites for this drug in phospholipid membranes. More specifically, acidic phospholipids retain siramesine on the bilayer surface due to a high-affinity interaction, reaching saturation at an apparent 1:1 drug−acidic phospholipid stoichiometry, where after the drug penetrates into the hydrocarbon core of the membrane. This behavior was confirmed using Langmuir films. Of the anionic phospholipids, the highest affinity, comparable to the affinities for the binding of small molecule ligands to proteins, was measured for phosphatidic acid (PA, mole fraction of $X_{PA} = 0.2$ in phosphatidylcholine vesicles), yielding a molecular partition coefficient of $240 \pm 80 \times 10^6$. An MD simulation on the siramesine:PA interaction was in agreement with the above data. Taking into account the key role of PA as a signaling molecule promoting cell growth our results suggest a new paradigm for the development of anticancer drugs, viz. design of small molecules specifically scavenging phospholipids involved in the signaling cascades controlling cell behavior.

## Introduction

Siramesine (1′-[4-[1-(4-fluorophenyl)-1*H*-indol-3-yl]-1-butyl]-spiro[isobenzofuran-1(3*H*),4′-piperidine], SRM, Figure 1) was originally synthesized by H. Lundbeck A/S for treatment of anxiety.

Phase II trials showed this compound to be nontoxic and well tolerated in humans. However, the clinical efficacy was not satisfactory, and its development was discontinued in 2002.[1] The primary target of SRM has been suggested to be the $\sigma-2$ receptor,[2] an orphan with no endogenous ligand known. These receptors have unique drug interaction profiles binding, for instance, haloperidol and sertraline, and their activity has been associated with various psychiatric disorders.[3] The physiological functions of $\sigma$ receptors remain unknown. The $\sigma-1$ receptor has been cloned, whereas the $\sigma-2$ receptor still needs to be isolated.[4] The latter have been found to be associated with the so-called lipid rafts.[5] Interestingly, $\sigma$ receptors are abundant in

many malignant cells, and there is evidence suggesting their crucial role in cell proliferation.[6] Along these lines, SRM has been recently demonstrated to suppress growth of several cell lines in vitro, and it has also been shown to inhibit growth of solid tumors in mice.[7]

Several drugs used to treat psychiatric disorders and cancer (e.g., haloperidol, chlorpromazine, clozapine, and doxorubicin) bind avidly to phospholipids, acidic phospholipids in particular.[8,9] We studied the interactions of SRM with model biomembranes composed of zwitterionic and anionic phospholipids using fluorescence spectroscopy (employing the intrinsic fluorescence of SRM as well as different fluorescent lipid analogs), DSC, Langmuir balance, and molecular dynamics (MD) simulations. Our results demonstrate a high-affinity binding of SRM to phosphatidic acid. This interaction is discussed in the context of the role of this phospholipid

[†] University of Helsinki.
[‡] MEMPHYS-Center for Biomembrane Physics, University of Southern Denmark.
[§] University of Reading.
[||] Nucleic Acids Center, University of Southern Denmark.
[⊥] Danish Cancer Society.
(1) Heading, C. *Curr. Opin. Invest. Drugs* **2001**, *2*, 266–270.
(2) Soby, K. K.; Mikkelsen, J. D.; Meier, E.; Thomsen, C. *Neuropharmacology* **2002**, *43*, 95–100.
(3) Guitart, X.; Codony, X.; Monroy, X. *Psychopharmacology* **2004**, *174*, 301–319.
(4) Colabufo, N. A.; Berardi, F.; Abate, C.; Contino, M.; Niso, M.; Perrone, R. *J. Med. Chem.* **2006**, *49*, 4153–4158.

(5) Gebreselassie, D.; Bowen, W. D. *Eur. J. Pharmacol.* **2004**, *493*, 19–28.
(6) Vilner, B. J.; John, C. S.; Bowen, W. D. *Cancer Res.* **1995**, *55*, 408–413.
(7) Ostenfeld, M. S.; Fehrenbacher, N.; Høyer-Hansen, M.; Thomsen, C.; Farkas, T.; Jäättelä, M. *Cancer Res.* **2005**, *65*, 8975–8983.
(8) Jutila, A.; Söderlund, T.; Pakkanen, A. L.; Huttunen, M.; Kinnunen, P. K. J. *Chem. Phys. Lipids* **2001**, *112*, 151–163.
(9) Söderlund, T.; Jutila, A.; Kinnunen, P. K. J. *Biophys. J.* **1999**, *76*, 896–907.
(10) Coon, M.; Ball, A.; Pound, J.; Ap, S.; Hollenback, D.; White, T.; Tulinsky, J.; Bonham, L.; Morrison, D. K.; Finney, R.; Singer, J. W. *Mol. Cancer Ther.* **2003**, *2*, 1067–1078.
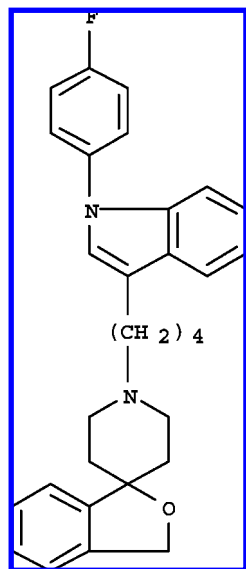
**Figure 1.** Chemical structure of siramesine (SRM).

as a second messenger promoting cell growth, allowing cancer cells to escape apoptosis.[10,11]

## Materials and Methods

**Chemicals.** 1-Palmitoyl-2-oleoyl-*sn*-glycero-3-phosphocholine (POPC), 1-palmitoyl-2-oleoyl-*sn*-glycero-3-(phospho-L-serine) (POPS), 1-palmitoyl-2-oleoyl-*sn*-glycero-3-phospho-*rac*-glycerol (POPG), 1-palmitoyl-2-oleoyl-*sn*-glycerol-3-phosphoethanolamine (POPE), 1-palmitoyl-2-oleoyl-*sn*-glycero-3-phosphoinositol (POPI), 1,2-dipalmitoyl-*sn*-glycero-3-phospho[*N*-(4-nitrobenz-2-oxa-1,3-diazolyl)]ethanolamine (DPPN), 1,2-dioleyl-*sn*-glycero-3-phosphoethanol (DOPet), 1,2-dioleyl-*sn*-glycero-3-phosphomethanol (DOPmet), 1-stearoyl-2-hydroxy-*sn*-glycero-3-phosphate (Lyso-PA), and 1-stearoyl-2-hydroxy-*sn*-glycero-3-[phospho-*rac*-(1-glycerol)] (Lyso-PG) were from Avanti Polar Lipids (Alabaster, AL). 1-Palmitoyl-2-[10-(pyren-1-yl)]decanoyl-*sn*-glycero-3-phosphocholine (PPDPC) was from K&V Bioware (Espoo, Finland). SRM was kindly provided by H. Lundbeck A/S (Copenhagen, Denmark). Deionized Milli-Q (Millipore, Bedford, MA) filtered water was used in all experiments. Hepes, NaCl, EDTA, and egg yolk-phosphatidic acid (egg-PA) were from Sigma. All chemicals were of analytical purity. The lipids were analyzed by thin layer chromatography on silicic acid coated plates, developed with chloroform/methanol/water/ammonia (65/20/2/2, by volume) as the solvent. No impurities were detected upon examination upon UV illumination or after iodine staining.

Lipid and drug concentrations were determined gravimetrically using a high-precision microbalance (Cahn Instruments Inc., Cerritos, CA). The concentrations of PPDPC and DPPN were determined from their absorption spectra (Cary-100 Bio, Varian Inc., Victoria, Australia) recorded using quartz cuvettes with a 1 cm path length and employing 42 000 cm$^{-1}$ at 342 nm and 21 000 cm$^{-1}$ at 463 nm as their molar extinction coefficients, respectively. A stock solution of SRM was made in chloroform. Proper aliquots were dried under a gentle flow of N$_2$, and the dry residue was dissolved in dimethylsulfoxide (DMSO, Merck) or ethanol, as indicated. The molar absorptivity of SRM was 20 000 cm$^{-1}$ at 258 nm, determined from its absorption spectra recorded for a 10 μM solution in ethanol.

**Preparation of Liposomes.** Lipids were dissolved in chloroform and subsequently mixed in this solvent so as to obtain the desired compositions. The solvent was removed using a gentle stream of nitrogen where after the dry lipid residues were maintained under reduced pressure for at least 2 h in order to remove trace amounts of chloroform. The lipids were hydrated into 20 mM Hepes, 0.1 mM EDTA, pH 7.0. During hydration the dispersing was aided by

a shaking water bath at room temperature so as to yield multilamellar vesicles. Large unilamellar vesicles (LUV) were prepared by extrusion using a LiposoFast (Avestin, Ottawa, Canada) small-volume homogenizer. The lipid dispersions were passed 19 times through polycarbonate filters with an average pore diameter of 100 nm (Millipore, Bedford, MA) in order to yield LUVs with an average diameter of 80 ± 25 nm.[12]

**Fluorescence Spectroscopy.** Steady-state fluorescence spectra were measured in four-window quartz cuvettes with a 1 cm path length using a fluorescence spectrophotometer (LS-50B, Perkin-Elmer, MA) equipped with a thermostatted temperature-controlled cuvette holder. For excitation of SRM, 254 nm was used, corresponding to its absorption maximum, with emission collected from 300 to 500 nm. Emission and excitation band passes were set at 5 nm. Measurements were conducted at 25 °C. For following the binding kinetics a time drive of 40 min was used. The intensity values used for the plots were taken at 10 min after drug addition. As a negative control SRM was added into the buffer without lipids.

**Determination of cmc.** The critical micelle concentration (cmc) for SRM was determined at ambient temperature (approximately 22 °C) with an 8-channel surface tension platereader (Delta-8, Kibron Inc., Espoo, Finland). For these measurements serial dilutions prepared in 96-well plates (DynePlates, Kibron) in the indicated concentration range were employed. These data were analyzed utilizing the Gibbs adsorption isotherm embedded in the dedicated software from the instrument manufacturer (Delta-8 Manager).

**Binding of SRM to Liposomes.** Siramesine−liposome interactions were assessed by steady-state fluorescence spectroscopy and fluorescently labeled lipids. These assays were conducted in quartz cuvettes and a spectrofluorometer (Cary Eclipse, Varian Inc., Victoria, Australia) equipped with a four-position Peltier element thermostatted cuvette holder. Excitation was set at 344 and 465 nm, corresponding to the absorption maxima of PPDPC and DPPN, respectively. Emission was collected in the range of 370−500 nm, allowing detection of the monomer peak of pyrene at 398 nm and 485−600 nm for emission of DPPN with a maximum at 535 nm. The emission and excitation band passes were both set at either 5 or 10 nm for PPDPC or DPPN, respectively.

The molar partition coefficients for the binding of SRM to liposomes with different lipid compositions were quantitated as described previously.[13] In brief, quenching of a fluorescent lipid analog by SRM and subsequent reversal of quenching by unlabeled liposomes were analyzed using two titrations. First, [lipid] was maintained constant while increasing [drug]; subsequently, [drug] was kept constant and [lipid] progressively increased with constant concentration of the fluorophore. On the basis of the assumption that at equilibrium the mole fraction of the drug partitioning into a bilayer of the given lipid composition causes similar relative quenching irrespective of the total [lipid] or [drug], we can calculate the partition coefficient for the drug.

**Binding of SRM to Lipid Monolayers.** Penetration of SRM into monomolecular lipid films was measured using a Langmuir tensiometer (DeltaPi, Kibron Inc., Espoo, Finland) with magnetically stirred circular wells with a subphase volume of 1.2 mL (Multiwell plate, Kibron Inc.). Surface pressure π was monitored with a metal alloy probe hanging from a high-precision microbalance (KBN129, Kibron Inc.). The indicated lipids were mixed in chloroform (*c* = 1 mM) and spread on the air−water interface using a microsyringe. The monolayers were allowed to equilibrate for 5−15 min to reach the indicated initial surface pressure values (π$_0$). A 4.8 μL amount of 0.4 mM SRM (dissolved in DMSO) was then

(11) Kim, J.; Lee, Y. H.; Kwon, T. K.; Chang, J. S.; Chung, K. C.; Min, D. S. *Cancer Res.* **2006**, *66*, 784–793.

(12) MacDonald, R. C.; MacDonald, R. I.; Menco, B. P.; Takeshita, K.; Subbarao, N. K.; Hu, L. R. *Biochim. Biophys. Acta* **1991**, *1061*, 297–303.

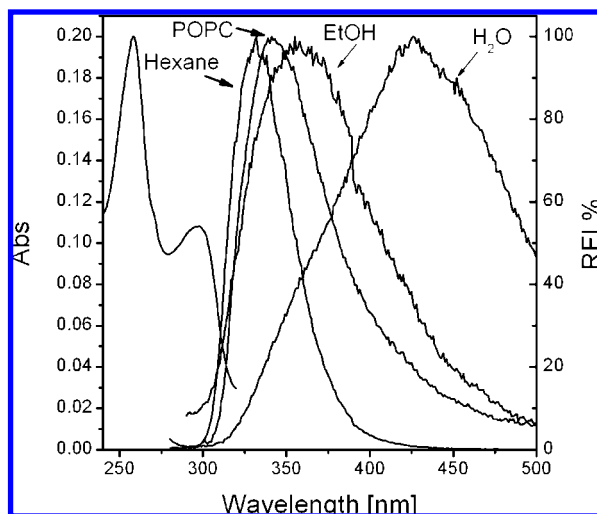(13) Parry, M. J.; Jutila, A.; Kinnunen, P. K. J.; Alakoskela, J. M. *J. Fluoresc.* **2007**, *17*, 97–103.

**Figure 2.** Absorption spectrum of 10 $\mu$M SRM in ethanol (left), and emission spectra (normalized at RFI = 100) in hexane, ethanol, buffer (20 mM Hepes, 0.1 mM EDTA pH 7.0), and with 20 $\mu$M POPC vesicles, as indicated. All spectra were recorded with the drug added in a small volume (2 $\mu$L, total volume 2 mL) of chloroform yielding final [SRM] = 10 $\mu$M in ethanol and [SRM] = 6 $\mu$M in buffer and with liposomes. $T$ = 25 °C.



**Figure 3.** Adsorption isotherm of SRM on 20 mM Hepes, 0.1 mM EDTA, pH 7.0 buffer measured at room temperature (approximately 22 °C). The error bars represent standard deviations for two consecutive measurements.

injected the subphase (20 mM Hepes, 0.1 mM EDTA, pH 7.0) to yield a final drug concentration of 1.6 $\mu$M. This amount of DMSO as such had no effect on the surface pressure. The difference between $\pi_0$ and the final surface pressure after addition of drug was taken as the increase in surface pressure ($\Delta\pi$). The data are represented as $\Delta\pi$ vs $\pi_0$, thus revealing the effect of increased lateral packing on penetration of the drug into the monolayer.[14]

**Differential Scanning Calorimetry (DSC).** The indicated amounts of the drug and lipids were mixed in chloroform. These mixtures were dried under a stream of nitrogen and subsequently kept under reduced pressure for at least 2 h to remove traces of the solvent. The samples were hydrated in 20 mM Hepes, 0.1 mM EDTA, pH 7 at 60 °C for 30 min in a shaking water bath as to yield multilamellar liposomes utilized in the DSC measurements. The samples, final lipid concentration 0.4 mM, were equilibrated on an ice water bath for at least 10 h to ensure equal thermal histories. The endotherms were recorded using a microcalorimeter (VP-DSC, Microcal Inc., Northampton, MA) at a heating rate of 30°/h. All scans were repeated to ensure their reproducibility. Deviation from the baseline was taken as the beginning of the transition and return to the baseline as its end. The endotherms were analyzed using the routines of the software provided by the instrument manufacturer.

**Molecular Dynamics (MD) Simulations.** MD simulations of SRM were implemented in lipid bilayers of three different compositions, viz. (i) pure POPC, (ii) POPC with a mole fraction $X_{maPA}$ = 0.20 of monoanionic PA (maPA), and (iii) POPC with a mole fraction $X_{daPA}$ = 0.20 of dianionic PA (daPA). For the sake of brevity, these simulations will be referred to as POPC, maPA, and daPA, respectively. The simulations were carried out with SRM protonated at the tertiary nitrogen. The distribution of partial charges near this site is shown in Figure S1, Supporting Information. PA molecules were uniformly distributed in each 64-lipid bilayer leaflet. Eight molecules of SRM, corresponding to an SRM:PA ratio of ~1:3, were added to each hydrated bilayer. Four SRM molecules were placed 10 Å away from the surface of one bilayer leaflet, while the other four were placed vicinal to the surface of the other, adjacent leaflet. All SRM molecules were initially randomly oriented with respect to the bilayer normal (Figure 2). Sodium and chloride ions were added as necessary to keep the system electrically neutral. MD simulations were carried out using the GROMACS 3.3.1
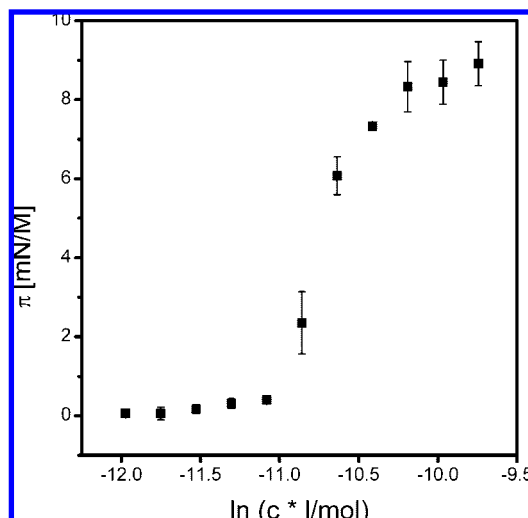
package.[15] Details of the simulation parameters and force field parametrization of maPA, daPA, and SRM are provided in the Supporting Information.

The simulations were carried out for ~90 ns for each system, which was sufficient for SRM molecules to partition into the bilayers and attain equilibrium conformations. The first 40 ns were discarded as equilibration time when calculating average properties.

## Results

As expected from its chemical structure (Figure 1) SRM is fluorescent. In ethanol it has absorption bands at 258 and 297 nm, and upon excitation at 258 nm a broad emission band peaking at 356 nm is seen (Figure 2). The emission intensity was significantly reduced in water with a weak band centered at 425 nm (Figure 2).

Further anticipated from its chemical structure SRM is amphiphilic as demonstrated by its partitioning into the air/water interface (Figure 3). The recorded isotherm yields 37 ± 6.7 Å$^2$ as the interfacial area of SRM, with cmc observed at 32 ± 1.2 $\mu$M. As expected from the above, SRM partitions efficiently into phosphatidylcholine liposomes with a significant increase seen in its quantum yield together with a 4 nm blue shift in the peak wavelength (Figure 2), suggesting SRM becomes accommodated in a nonpolar environment, in the hydrocarbon region of the bilayer.

Kinetics of the binding of SRM to liposomes revealed this process to be biphasic with an initial fast (approximately 15 s) and pronounced increase in fluorescence being followed by a slower, smaller decrease in intensity (data not shown). As already demonstrated for several other membrane associating cationic drugs,[8,16] anionic phospholipids promote binding of SRM to bilayers. Accordingly, increasing the content of phosphatidylserine $X_{PS}$ in liposomes caused a marked increase in the membrane binding of SRM as reflected by a pronounced increase in its fluorescence (Figure 4). The presence of 150 mM NaCl diminished the binding of SRM to LUVs with progressively less effect upon increasing $X_{PS}$, thus also

(14) Brockman, H. *Curr. Opin. Struct. Biol.* **1999**, *9*, 438–443.

(15) Lindahl, E.; Hess, B.; van der Spoel, D. *J. Mol. Model.* **2001**, *7*, 306–317.

(16) Jutila, A.; Rytömaa, M.; Kinnunen, P. K. J. *Mol. Pharmacol.* **1998**, *54*, 722–732.
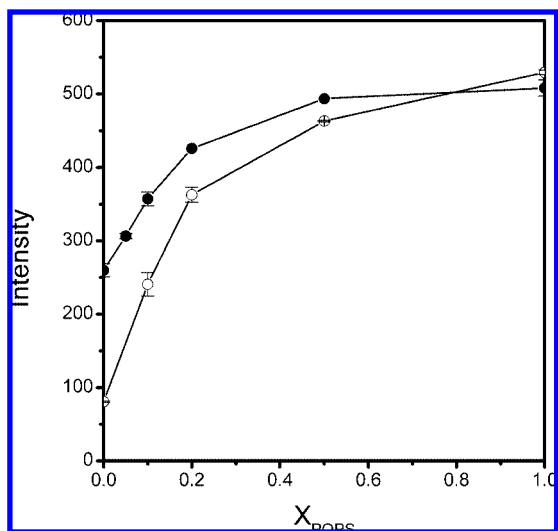
**Figure 4.** Change in the fluorescence intensity of SRM added to liposomes with increasing contents of the anionic POPS (●), in buffer and in the presence of 150 mM NaCl (○). [SRM] = 2.5 $\mu$M corresponding to drug:phospholipid stoichiometry of 1:8. The values for fluorescence intensity were taken 10 min after drug addition. Excitation at 254 nm and emission at 350 nm. $T$ = 25 °C. Spectra were recorded in 20 mM Hepes, 0.1 mM EDTA, pH 7.0, total [lipid] = 20 $\mu$M.

revealing electrostatics to contribute to the association of SRM to membranes containing this negatively charged phospholipid.

In order to study the localization of SRM in liposomes we used SRM as a quencher for trace amounts of different fluorescent lipid analogs. We first employed PPDPC, a phospholipid analog containing a pyrene-decanoyl chain in the *sn*-2 position. As there is no spectral overlap between SRM and pyrene the observed quenching (Figure 5) is collisional, reflecting efficient binding of SRM to POPC vesicles and causing at a drug:phospholipid ratio of 1:2 a maximally 60% decrement in PPDPC emission. While the hydrophobicity of the pyrene moiety of PPDPC causes this fluorophore to reside in the hydrocarbon region of the membrane, its polarizability together with cation−$\pi$ interactions should prefer a more interfacial orientation.[17,18] Interestingly, including PS ($X$ = 0.50) to the vesicles attenuated the quenching of PPDPC by SRM (Figure 5) and increasing the content of PS further to $X$ = 0.99 augmented this effect with only a minor decrement caused by SRM in PPDPC fluorescence. For vesicles with $X_{PS}$ = 0.2 the quenching was biphasic with the initial small decrement in fluorescence caused by 4 $\mu$M SRM (corresponding to an apparent drug:PS molar ratio of 1:1) being followed by a progressive and pronounced quenching upon further increase in [drug]. This was further elucidated for vesicles with $X_{PA}$ = 0.02, 0.05, 0.10, and 0.20. Similarly to $X_{PS}$ = 0.2 quenching was biphasic (Figure 5B) with the discontinuity observed at SRM concentrations varying linearly with $X_{PA}$ and corresponding to an apparent 1:1 drug:PA molar ratio. The above data suggest formation of stoichiometric complexes by SRM and PA on the membrane surface, preventing penetration of SRM into the membrane hydrocarbon region where the pyrene moiety of PPDPC is accommodated.

(17) Hoff, B.; Strandberg, E.; Ulrich, A.; Tieleman, D.; Posten, C. *Biophys. J.* **2005**, *88*, 1818–1827.
(18) Yau, W.; Wimley, W.; Gawrisch, K.; White, S. *Biochemistry* **1998**, *37*, 14713–14718.

Subsequently, we used another lipid analog DPPN bearing a fluorescent NBD label in the headgroup. For this probe ($X$ = 0.01) and POPC vesicles, the decrement in fluorescence caused by 4 $\mu$M SRM was 50% (Figure 6), and efficient quenching was observed also for PS containing LUVs ($X_{PS}$ = 0.20) with little difference when compared to neat POPC LUVs.

To compare the affinities of SRM to different phospholipids we determined the partition coefficients for SRM between the aqueous solution and vesicles containing POPC, POPS, POPG, egg-PA, Brain-PI, POPE, DOPMe, DOPet, lyso-PA, and lyso-PG using the headgroup labeled DPPN ($X$ = 0.01) as a fluorophore (Table 1). In keeping with the above fluorescence studies SRM preferentially binds to acidic lipids with the highest affinity $K_P = 240 \pm 80 \times 10^6$ measured for PA.

To further assess the specificity of the binding and preference of different cationic amphiphilic drugs for anionic phospholipids we determined the partitioning of chlorpromazine, doxorubicin, clozapine, and haloperidol to vesicles containing PG, PA, or PS. The highest affinities of the above drugs were measured for PS followed by PG, while the lowest affinity was observed for PA-containing vesicles (Table 2).

The above quenching experiments suggest that SRM intercalates into the hydrocarbon region of neat POPC bilayers, while in the presence of anionic lipids two modes of binding are evident: a high-affinity binding site in the membrane surface with SRM bound to the acidic phospholipid headgroup and a second site with the drug intercalating into the hydrocarbon region. To verify the above conclusions from the fluorescence quenching experiments study we measured the penetration of SRM into lipid monolayers residing on the air/buffer interface (Figure 7). In accordance with the above fluorescence data a pronounced increase in surface pressure due to SRM added into the subphase was observed for pure PC films, while $X_{PS}$ = 0.2 dramatically decreased the penetration. This readily complies with an interfacial location of SRM in films containing the acidic phospholipid. Intriguingly, the association of SRM to monolayers containing PA is different from those with PS (Figure 7) with high values for $\Delta\pi$ being measured. This is most likely caused by the more extensive partitioning of SRM to PA together with a pronounced relative increase in the effective headgroup size of this lipid upon binding of SRM.

The impact of SRM on the thermal phase behavior of liposomes studied by DSC is in keeping with the above data (see Supporting Information Figure S3). The main phase transition temperature $T_m$ decreases as a function of $X_{SRM}$ with broadening of the peak to lower temperatures for DPPC MLVs. The pretransition temperature $T_p$ decreases, and at $X_{SRM}$ = 0.05 the pretransition disappears, in keeping with the perturbation caused by the drug in the hydrocarbon region of the bilayer (Supporting Information Figure S4).

The main conclusions from the above experiments could be substantiated in MD simulations. Accordingly, SRM molecules partitioned into the bilayer phase within 30 ns in all simulations. The equilibrium distribution of the drug along the bilayer normal is shown in Figure 8. The depth of penetration was largest for POPC and lowest for daPA with the average distance between SRM and the bilayer center along the bilayer normal being 11.88 ± 1.32, 14.83 ± 1.40, and 15.22 ± 2.25 Å for POPC, maPA, and daPA, respectively. Thus, SRM intercalated deeper into the hydrocarbon core of POPC, even at a low SRM:PA molar ratio of 1:3, in agreement with the fluorescence quenching data.
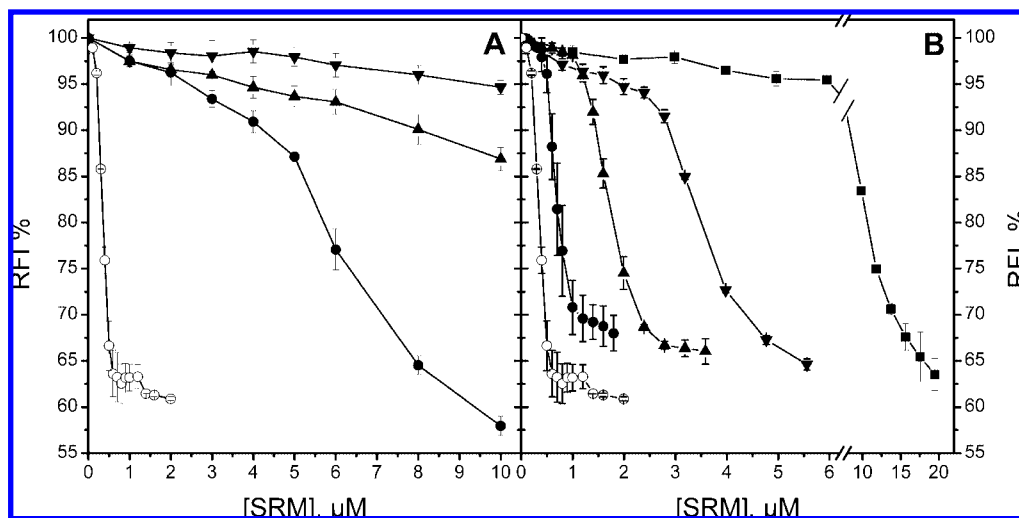
**Figure 5.** Quenching by SRM of the pyrene-labeled phospholipid analog PPDPC ($X = 0.01$) in POPC vesicles: (A) with $X_{POPS} = 0$ (○), 0.20 (●), 0.50 (▲), and 0.99 (▼) and (B) $X_{PA} = 0$ (○), 0.02 (●), 0.05 (▲), 0.10 (▼), and 0.20 (■). Total phospholipid was 20 $\mu$M in 20 mM HEPES, 0.1 mM EDTA, pH 7.0, $T = 25$ °C.
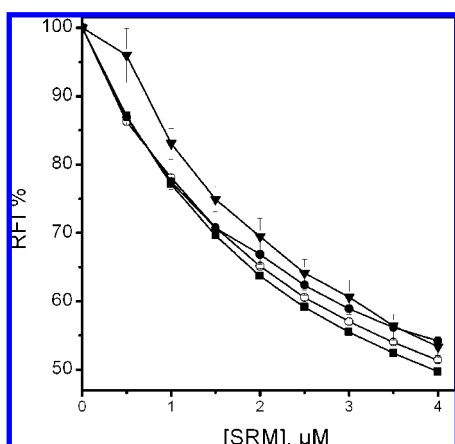


**Figure 6.** Quenching of DPPN ($X = 0.01$) fluorescence by SRM in POPC LUVs (○), LUVs containing $X_{PS} = 0.2$ (●), $X_{PS} = 0.99$ (▼), and $X_{PA} = 0.2$ (■). The error bars represent the standard deviation of at least two consecutive measurements. Conditions as described in the legend for Figure 5.

**Table 1.** Molar Partition Coefficients for the Binding of Siramesine to Liposomes

| lipid composition | $K_p/10^6$ |
|---|---|
| $X_{LIPID} = 1.0$ | |
| POPC | 1.2 ± 0.09 |
| POPS | 2.1362 ± 0.0004 |
| POPG | 120 ± 64 |
| $X_{PC} = 0.8$ | |
| POPC/POPE | 1.15 ± 0.04 |
| POPC/POPS | 3.3 ± 0.4 |
| POPC/Lyso-PG | 5.0 ± 0.4 |
| POPC/Lyso-PA | 7.2 ± 0.2 |
| POPC/DOPEt | 8.2 ± 0.7 |
| POPC/POPG | 9.4 ± 2.1 |
| POPC/DOPMe | 9.9 ± 1.1 |
| POPC/POPI | 29 ± 3 |
| POPC/egg-PA | 240 ± 80 |

The strongest interactions of PA with SRM were with the protonated nitrogen of SRM. Figure 9 shows the radial distribution functions (RDF) of the protonated nitrogen ($N_p$) of SRM with the two possible hydrogen-bonding sites on PA, i.e., the

**Table 2.** Molar Partition Coefficients ($K_p/10^6$) for Binding of the Indicated Cationic Amphiphilic Drugs to Liposomes Containing Different Anionic Phospholipids; Siramesine Is Included for Comparison

| | liposomes (PS, PG, or PA, $X = 0.2$) | | |
|---|---|---|---|
| drug | POPC/egg-PA | POPC/POPS | POPC/POPG |
| doxorubicin | 1.21 ± 0.01 | 2.96 ± 0.35 | 1.92 ± 0.07 |
| chlorpromazine | 5.96 ± 0.65 | 23.7 ± 5.79 | 13.89 ± 3.77 |
| clozapine | 2.77 ± 0.21 | 11.16 ± 4.01 | 3.33 ± 0 |
| haloperidol | 5.5 ± 3.76 | 2.02 ± 1.47 | 11.97 ± 4.04 |
| siramesine | 240 ± 80 | 3.3 ± 0.4 | 9.4 ± 2.1 |

phosphate ($PO_4^-$) moiety and the ester group. The higher negative charge density of ($PO_4^-$) resulted in a strong N−H−O−P hydrogen bonding between the SRM $N_p$ and the ($PO_4^-$) oxygen atoms. This H bonding was present in both maPA and daPA but stronger in the latter. In daPA, the higher charge (−2) also caused formation of an SRM aggregate near
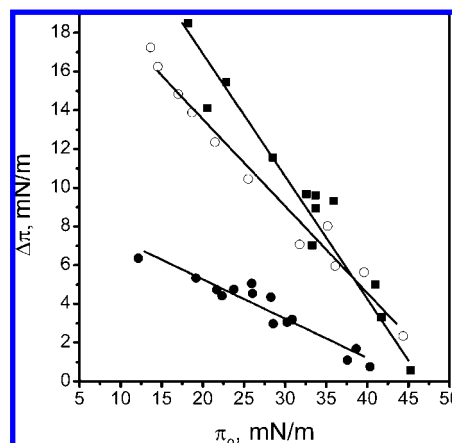


**Figure 7.** Intercalation of SRM into phospholipid monolayers. SRM (1.6 $\mu$M) added into the subphase and the increase in surface pressure $\Delta\pi$ vs initial surface pressure $\pi_0$ was recorded. The films were composed of POPC (○), POPC with POPS ($X = 0.2$ (●)), and POPC with egg-PA ($X = 0.20$ (■)). The lines represent linear fits to the data.
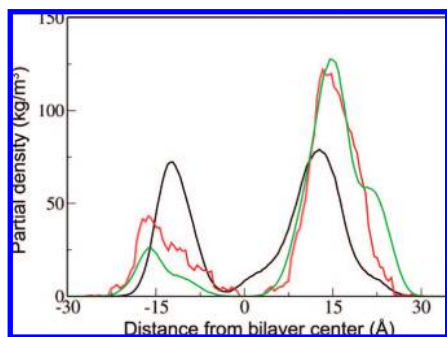
**Figure 8.** Equilibrium distribution of SRM into the three different bilayers with data from maPA (red line) and daPA (green line) simulations superimposed on the SRM distribution in the POPC simulation (black line). The bilayer center is at $z = 0$.

the interface, which could prevent SRM from penetrating deeper into the bilayer.

## Discussion

Effects of drugs are conventionally rationalized in terms of small molecule ligand−receptor protein interactions. However, there are recent data suggesting that several drugs partition efficiently into membrane lipids and affect both membrane organization and dynamics, thus influencing indirectly the environment and conformation of ion channels and receptors as well as other membrane-embedded proteins.[9,19−21] Several drugs associating with acidic phospholipids have been further demonstrated to displace in a competitive manner peripheral proteins from membranes.[16] Drug−phospholipid complex formation may also underlie toxic side effects, as exemplified by phospholipidosis, the intracellular accumulation of phospholipids resulting in inhibition of phospholipases and changes in phospholipid synthesis.[22,23]

Notably, clinically relevant effects of drugs are commonly observed at far lower drug concentrations than changes in membrane properties. Accordingly, the high and apparently quite specific affinity of SRM to PA is unprecedented. More specifically, our data demonstrate that while SRM partitions into the hydrocarbon region of zwitterionic PC membranes, in the presence of negatively charged phospholipids, PA in particular, it is very efficiently retained in the interface (Figure 8), apparently forming a complex with acidic phospholipids. The affinity of SRM to phosphatidic acid was found to be high, its partitioning into membranes with $X_{PA} = 0.20$ being of an order of magnitude higher as compared to membranes with an equal content of other acidic phospholipids (Table 1; Figure 10). The measured partition coefficient $K_p = 240 \pm 80 \times 10^6$ corresponds to a dissociation constant of approximately 0.23 $\mu$M, which is comparable to the affinities reported for small molecule ligand−macromolecule interactions as measured for doxorubicin and DNA ($K_d = 68 \ \mu M^{24}$) and for the binding of clozapine to the dopaminergic D2 receptor ($K_d = 44$ nM[25]). The high-affinity binding to PA seems to be specific with little correlation to

factors such as headgroup size or dipole potential (as measured by di-8-ANEPPS, data not shown).

With the above data providing evidence for SRM-PA complex formation, we performed MD simulations to reveal potential modes of interaction. It has been suggested that upon hydrogen-bond formation with a charged amine PA would be deprotonated into a divalent anion, yielding daPA.[26,27] This could be involved also in the SRM-PA complex formation, favoring electrostatic interactions with the positive charge of SRM. In keeping with the above, MD simulations suggest that the binding of SRM to PA is driven by strong, electrostatically driven H-bond formation between $N_p$ and the negatively charged unshielded ($PO_4^-$) moiety of PA. The strength of this H bonding was sufficient to retain SRM near the interface in simulations on bilayers containing PA. Intriguingly, aggregation of SRM was observed when daPA is included in the bilayer. The interactions between $N_p$ of SRM and the lipid headgroup phosphate were evident also for neat POPC but weaker than for daPA (data not shown), thus allowing deeper penetration of SRM into the bilayer. A more detailed MD study involving simulations at progressively increasing SRM:lipid ratios is needed to comply with the quenching and monolayer data, in particular to address the exact stoichiometry of the complex.

PA has been assigned a central role as a secondary messenger in the regulation of various cellular functions. A number of proteins promoting cell survival, such as Hsp,[28] mTOR,[29] Raf,[30] Ras,[31] and Sos,[32] require PA for their activity. Yet, it is crucial also in the activation of RAS- and TNF-$\alpha$-mediated apoptosis.[33] PA may further be involved in the pathogenesis of systemic vasculitis.[34] The major pathway producing PA in vitro involves phospholipase D, which cleaves the headgroup of either PE or PC to yield PA. Other pathways producing PA in cells involve acylating lyso-PA by lyso-PA acyl transferase[35] and phosphorylation of diglyceride by diglyceride kinase.[36] Different cancer cell lines utilize distinct pathways to generate PA, allowing them to escape apoptosis,[37] and also exogenous PA has been shown to act as an antiapoptotic signal. Consequently, there is an intense search for PLD inhibitors that could be used as anticancer drugs to decrease the levels of cellular PA.

The role of PA in cell survival may also provide a mechanism to explain the anticancer activity of SRM. The dissociation constant for SRM to the $\sigma$ receptor is 1.1 nM[2], while the concentrations required for anticancer effect are in the range

(19) Cantor, R. S. *Toxicol. Lett.* **1998**, *100−101*, 451−458.
(20) Alakoskela, J. M.; Söderlund, T.; Holopainen, J. M.; Kinnunen, P. K. J. *Mol. Pharmacol.* **2004**, *66*, 161−168.
(21) Mattila, J. P.; Sabatini, K.; Kinnunen, P. K. J. *Biophys. J.* **2007**, *93*, 3105−3112.
(22) Reasor, M. J.; Kacew, S. *Exp. Biol. Med.* **2001**, *226*, 825−830.
(23) Vitovic, P.; Alakoskela, J. M.; Kinnunen, P. K. J. *J. Med. Chem.* **2008**, *51*, 1842−1848.
(24) Bible, K. C. *Cancer Res.* **2000**, *60*, 2419−2428.
(25) Seeman, P. *Mol. Psychiatr.* **1998**, *3*, 123−134.

(26) Kooijman, E. E.; Carter, K. M.; van Laar, E. G.; Chupin, V.; Burger, K. N.; de Kruijff, B. *Biochemistry* **2005**, *44*, 17007−17015.
(27) Kooijman, E. E.; Tieleman, D. P.; Testerink, C.; Munnik, T.; Rijkers, D. T.; Burger, K. N.; de Kruijff, B. *J. Biol. Chem.* **2007**, *282*, 11356−11364.
(28) Chowdary, T. *Biochem. J.* **2007**, *401*, 437−445.
(29) Hornberger, T. A.; Chu, W. K.; Mak, Y. W.; Hsiung, J. W.; Huang, S. A.; Chien, S. *Proc. Natl. Acad. Sci. U. S. A.* **2006**, *103*, 4741−4746.
(30) Ghosh, S.; Strum, J. C.; Sciorra, V. A.; Daniel, L.; Bell, R. M. *J. Biol. Chem.* **1996**, *271*, 8472−8480.
(31) Andresen, B. *FEBS Lett.* **2002**, *531*, 65−68.
(32) Zhao, C. *Nat. Cell Biol.* **2007**, *9*, 707−712.
(33) Hancock, J. F. *Nat. Cell Biol.* **2007**, *9*, 615−617.
(34) Williams, J. *J. Am. Soc. Nephrol.* **2007**, *18*, 1112−1120.
(35) La Rosee, P.; Jia, T.; Demehri, S.; Hartel, N.; de Vries, P.; Bonham, L.; Hollenback, D.; Singer, J. W.; Melo, J. V.; Druker, B. J.; Deininger, M. W. *Clin. Cancer Res.* **2006**, *12*, 6540−6546.
(36) Sakane, F.; Imai, S.; Kai, M.; Yasuda, S.; Kanoh, H. *Biochim. Biophys. Acta* **2007**, *1771*, 793−806.
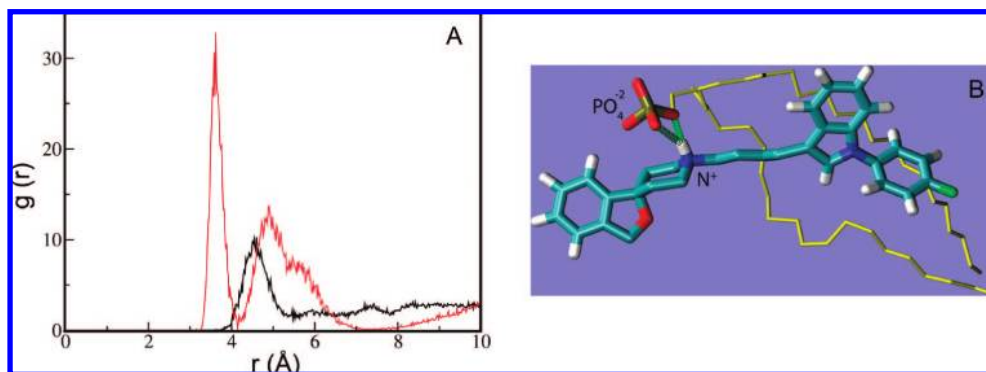(37) Steed, P. M.; Chow, A. H. *Curr. Pharm. Biotechnol.* **2001**, *2*, 241−256.

**Figure 9.** (A) Radial distribution functions between the protonated nitrogen of SRM and the headgroup atoms of maPA in the corresponding simulation. The phosphorus atom and ester carbon atoms were used for assigning the distribution with respect to the lipid phosphate (red line) and ester (black line) groups. (B) Simulation snapshot showing the H-bonding interaction between the SRM protonated nitrogen and the daPA phosphate group. The phosphorus and oxygen atoms of $PO_4^-$ are shown in gold and red, respectively, while SRM and the phosphate group are represented in licorice, and the rest of the lipid is shown in yellow. The hydrogen bonds are illustrated as green springs.
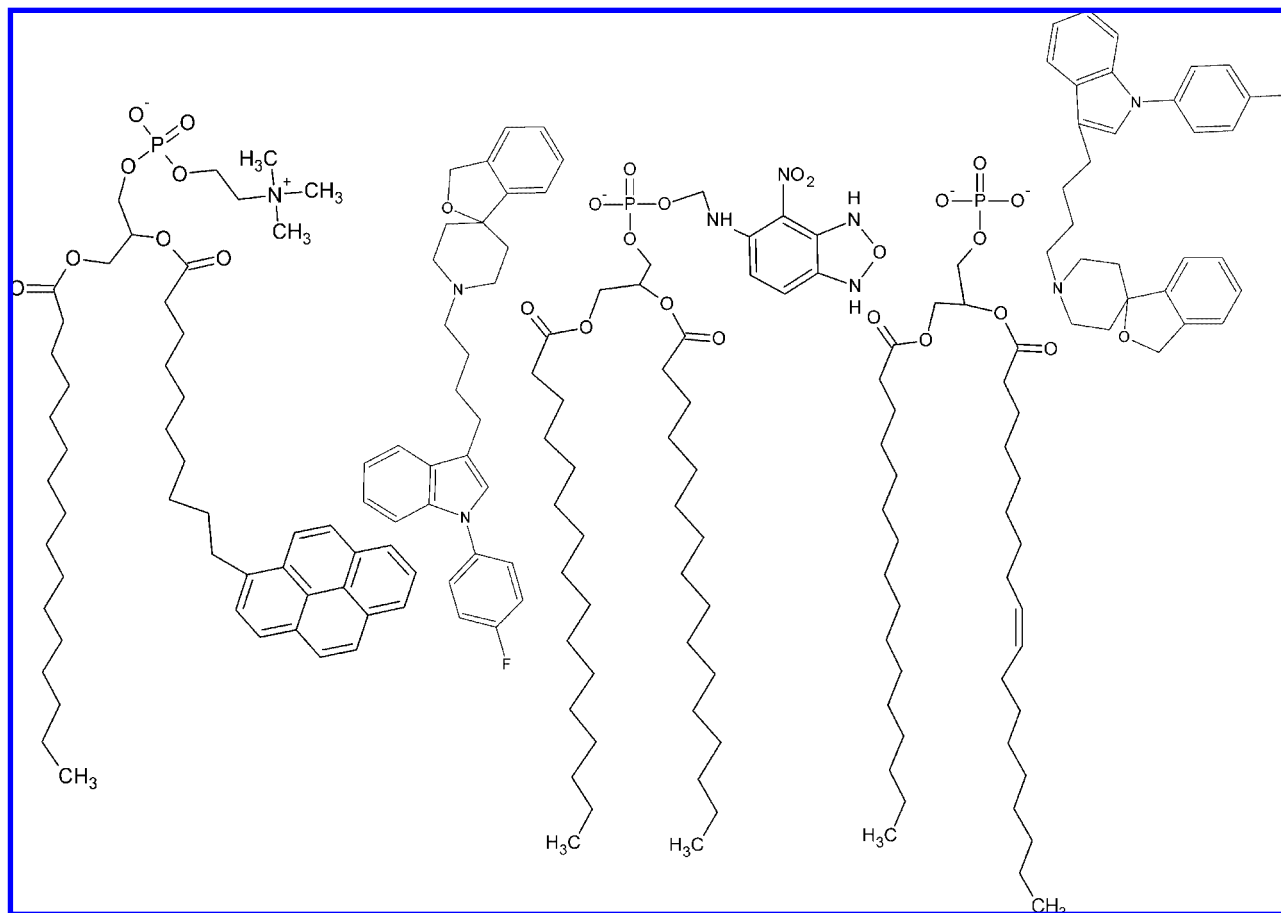


**Figure 10.** Schematic illustration of the relative position of membrane-bound SRM with respect to different fluorophores complying with the positional restrictions to collisional quenching in a bilayer leaflet. From left to right are depicted PPDPC, SRM, DPPN, and SRM-PA complex. On the left SRM is illustrated in an extended conformation, intercalated into the hydrocarbon region, quenching both the pyrene moiety of PPDPC and the NBD moiety of DPPN, respectively. In contrast, when bound to PA SRM is retained in the interface, quenching of only DPPN being possible.

of $1-2$ $\mu$M for cultured cells. For mice, assuming complete absorption, the applied dose roughly corresponds to a concentration of 14 $\mu$M,[38] suggesting that a great excess over the saturation of all the $\sigma$-binding sites was required. The concentrations needed for anticancer activity would thus suffice to have a significant occupancy of PA. Accordingly, sequestering of PA by SRM could impede proper functioning of proteins requiring this phospholipid for activity and thus

provide a simple molecular mechanism underlying the augmented apoptosis observed in cancer cells due to this drug.[7,38] While further structural analysis is needed to elucidate the exact nature of SRM-PA interaction, our data demonstrate that it is possible to generate small molecule drugs with affinity to a specific phospholipid species. Our findings potentially thus constitute a new paradigm of small

molecular anticancer drugs based on specific sequestering of lipid second messengers.

**Supporting Information Available:** Detailed information about the parameterization of the molecular dynamics simulations as well as data from the DSC measurements are given. This material is available free of charge via the Internet at http://pubs.acs.org.

JA800516W

(38) Groth-Pedersen, L.; Ostenfeld, M. S.; Høyer-Hansen, M.; Nylandsted, J.; Jäättelä, M. *Cancer Res.* **2007**, *67*, 2217–2225.